Biosensors and Bioelectronics 201 (2022) 113942

Contents lists available at ScienceDirect

Biosensors and Bioelectronics

journal homepage: www.elsevier.com/locate/bios

Plasmonic biosensor for the highly sensitive detection of microRNA-21 *via* the chemical etching of gold nanorods under a dark-field microscope

Qiang Zhang, Hong Hui Yan, Cheng Ru, Fu Zhu, Hong Yan Zou, Peng Fei Gao, Cheng Zhi Huang **, Jian Wang *

Key Laboratory of Luminescence Analysis and Molecular Sensing (Southwest University), Ministry of Education, And Key Laboratory of Luminescent and Real-Time Anal. Chem. (Southwest University), Chongqing Science and Technology Bureau, College of Pharmaceutical Sciences, Southwest University, Chongqing, 400715, PR China

ARTICLE INFO

Keywords:
MicroRNA-21
Strand displacement amplification
Dark-field image
Gold nanorods
Localized surface plasmon resonance

ABSTRACT

MicroRNAs involved in tumor-related tissues at abnormal expression level present tremendous potential in the early diagnosis of cancers. However, their intrinsic shortcomings, for instance, low abundance and high sequence homology, make it challengeable to quantify them with high sensitivity and selectivity. Herein, a highly sensitive platform with great specificity was developed for microRNA-21 based on the produced-I_2 triggered chemical etching of gold nanorods to a smaller size, resulting in a significant blue shift and a great intensity decrease in the localized surface plasmon resonance (LSPR) scattering. The synergism of strand displacement and enzymatic reaction enabled the proposed strategy with a high sensitivity and selectivity toward microRNA-21 in a dynamic range from 0.1 to 10,000 pM and a low limit of detection of 71.22 fM (3σ/k) by dark-field microscope. Additionally, the remarkable discrimination of single nucleotide difference suggested the superior selectivity towards microRNA-21, which presented a satisfactory recovery in human serum samples. The proposed plasmon platform could also serve as a universal and sensitive detection of cancer biomarkers, presenting the amusing application prospects in the early diagnosis of various cancers by adapting the corresponding nucleic acid sequences.

1. Introduction

MicroRNAs (miRNAs) play important roles in many biological processes and are associated with various diseases, especially cancers (Wu and Qu, 2015). Furthermore, the microRNAs involve in tumor-related tissues and expressed at abnormal level, which hold tremendous potential in the early diagnosis of cancers. However, due to the low abundance, short sequence, and high sequence similarity in their family, it makes the sensitive and selective detection of miRNAs face great challenges (Zhang et al., 2018).

To achieve the sensitive sensing of miRNAs, a wide range of traditional methods, including the reverse transcription polymerase chain reaction (Markou et al., 2008), northern blotting (Ouyang et al., 2019) *etc.*, have been developed with success, but the above mentioned methods require cumbersome steps with poor sensitivity, thus the simple and sensitive strategies for miRNAs detection are highly desirable and urgently needed. In order to address the issue of low abundance of miRNA in biological samples, a variety of nucleic acid signal amplification techniques have been developed for the sensitive miRNAs assays, including rolling circle amplification (Zhan et al., 2021), catalytic hairpin assembly (Liu et al., 2020a), hybrid chain reaction (Sun et al., 2020), strand displacement amplification (Li et al., 2018), *etc*. Especially, the strand displacement amplification (SDA) is a valid strategy for biosensors applications (Dai et al., 2019) due to the simple operation. Herein, a sensitive microRNA quantification strategy is proposed based on microRNA-triggered strand displacement reaction and the etching of gold nanorods (AuNRs) by produced-I_2 under a dark-field microscope.

To date, due to its outstanding spatial and temporal resolution, dark-field microscope (DFM) is a powerful tool to observe the optical imaging at single-particle level, which has been widely applied to the highly sensitive biochemical detection (Gao et al., 2021; Li et al., 2012), cell imaging (Liu et al., 2020b), and real-time reaction monitoring (Shi et al., 2013; Xu et al., 2020; Wang et al., 2019a). Furthermore, the dark-filed signal output presents in the form of light scattering intensity (Yan et al., 2021), color (Liu et al., 2020a) or counting (Tian et al., 2021; Li

* Corresponding author.
** Corresponding author.
E-mail addresses: chengzhi@swu.edu.cn (C.Z. Huang), wj123456@swu.edu.cn (J. Wang).

https://doi.org/10.1016/j.bios.2021.113942
Received 19 October 2021; Received in revised form 16 December 2021; Accepted 28 December 2021
Available online 31 December 2021

et al., 2017) of nanomaterials, which could be adjusted by means of assembly (Wang et al., 2021a), etching (Li et al., 2020; Wang et al., 2019b), and growth (Li et al., 2019) of nanomaterials.

Vigorous research efforts have advanced the state-of-the-art plasmonic nanomaterial with ultrahigh sensitivity for bioanalysis (Jin et al., 2020). Among them, AuNRs, as a fascinating light scattering optical probe have attracted increasing attention due to their unique localized surface plasmon resonance (LSPR) properties (Xianyu et al., 2021). Generally, the optical properties of AuNRs are closely related to their aspect ratio, surrounding environment, and assembly state, making it suitable for the biochemical detection (Liu et al., 2013) and intracellular imaging (Chen et al., 2015). For instance, Zhu group detected and imaged hydroxyl free radicals in living cells with AuNRs (Wu et al., 2020). Xu and her cooperators achieved the sensitive detection of tumor-related cancer biomarkers (microRNA-122) by combining with catalytic hairpin assembly as well as the hybrid chain amplification by monitoring the chemical etching of Ag coated AuNRs with the dark-field microscope (Zhao et al., 2019). In this work, a sensitive platform for quantifying microRNA-21 was developed by chemical etching of AuNRs. By the combination with strand displacement reaction and efficient magnetic separation, the specificity was satisfactory for microRNA-21 detection, which was effectively applied to human serum sample, suggesting the powerful potential in the field of early clinical diagnosis of diseases. What is more, this proposed strategy is a universal platform in detection of different miRNAs by replacing probe sequences, or changing the functionalized enzymes to realize various purposes.

2. Experiment section

The materials and reagents, instruments, preparation of AuNRs and the finite-difference time-domain (FDTD) simulation are shown in the Supporting Information, and the oligonucleotides sequences is listed in Table S1.

2.1. Preparation of enzyme-functionalized primers

According to the previous work (Fu et al., 2012), 3-(2-pyridinyldithio)-, 2, 5-dioxo-1-pyrrolidinylester (SPDP) was introduced to crosslink glucose oxidase (GOx) with the functionalized primers to form the GOx-DNA 1 conjugation, which was based on the reaction between lysine residues on the protein surface and amine-reactive *N*-hydroxysuccinimide (NHS) esters. Briefly, 100 μL of 2 mg/mL GOx reacted with 100 μL of SPDP (40 μM) in 1 × PBS (pH 7.4) at 37 °C for 2 h. And then, the excessive SPDP was allowed to wash and remove with 30 Kd cutoff filters. After the activation of the thiol-DNA 2 in dithiothreitol (DTT) solution (0.1 M) for 2 h, the activated DNA could further conjugate with the SPDP-modified protein by means of the exchange of a disulfide bond from the activated pyridyl dithiol group. Finally, the excessive DNA was removed with the same procedure as the removal of excessive SPDP. Finally, the UV-vis absorbance spectra were used for characterization of primers modified, which presented the obvious increase in absorbance at 343 nm (Fig. S1), suggesting that the functionalized GOx-DNA 1 was considered successfully obtained.

2.2. Probe preparation and strand displacement amplification assay

The preparation of probe included three produces. The first step was to assemble the biotin-DNA 1 conjugation onto the surface of the streptavidin-modified magnetic beads (MBs). 100 μL of 2 mg/mL MBs were washed three times with 1 × PBS buffer. After magnetic separation, the probe was resuspended with the same volume 1× PBS buffer. Then, 100 μL of biotin-DNA 1 was added into above mixture and gently shaken at 37 °C for 60 min, which was more negative charged (Fig. S2). Subsequently, the unattached biotin-DNA 1 was removed by magnetic separation and washed three times with 1 × PBS buffer.

The second step was DNA hybridization. 100 μL of GOx-DNA 2 (GOx conjugated with DNA 2) was mixed with 100 μL of MB-DNA 1 conjugation, and incubated at 37 °C for 60 min to hybrid. The excessive primer was subsequently removed by magnetic separation and washed three times with 1 × PBS buffer. And then, DNA hybridization double strands were resuspended in 200 μL of 1 × PBS buffer and stored at −20 °C for further application.

The third procedure was strand displacement amplification (Yan et al., 2021). 20 μL of DNA hybridization probe was obtained by the above protocol, which was mixed with 20 μL of target microRNA and 10 μL of fuel strand (10 μM), following by the gentle shaking and incubating at 37 °C for 2 h. After that, the solution supernatant was obtained by magnetic separation.

2.3. MiRNA-21 assay with DFM

50 μL of above supernatant was firstly reacted with 50 μL of glucose (500 mM) to produce H_2O_2, which was then mixed with 50 μL of KI (5.0 mM), 50 μL of HCl (50 mM) and 50 μL of AuNRs, following by the incubation at 25 °C for 20 min to etch AuNRs. After the chemical etching, AuNRs were deposited on the slide for 30 min, then were dried with nitrogen and covered with cover glass for imaging under the dark-field optical microscope with the exposure time for 200 ms. Finally, the light scattering intensity of AuNRs was collected by IPP software.

3. Results and discussion

3.1. The highly sensitive detection principle of microRNA-21

As shown in Scheme 1, the strategy for detection of miRNA including four steps. Firstly, streptavidin-modified MBs are assembled with biotin-DNA 1 to form MBs-DNA1 conjugation. Simultaneously, GOx is conjugated with DNA 2 to form enzyme-functionalized primer (GOx-DNA 2), then hybridized with MBs-DNA 1 to form complex probe. Secondly, the target microRNA-21 is involved in the strand displacement amplification with the aid of fuel strands to displace the GOx-DNA 2, which could be released to the solution after magnetic separation. Subsequently, H_2O_2 is produced when the released GOx-DNA 2 is mixed with glucose. Finally, AuNRs are chemically etched by KI and H_2O_2 under the acidic condition, which lead to the decrease in light scattering intensity of AuNRs. Importantly, the concentration of H_2O_2 is closed related to microRNA-21, which is highly relevant to with the decreased light scattering intensity of AuNRs.

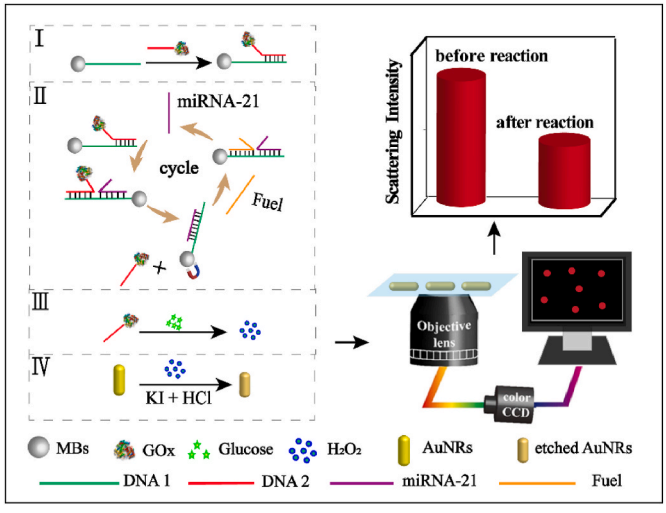

Scheme 1. Schematic diagram of high sensitivity detection of microRNA-21 with strand displacement amplification strategy under DFM.

3.2. The properties of light scattering optical probe

In this work, AuNRs acted as the light scattering optical probe, which presented the uniform cylindrical morphology with size about 79 × 30 nm (Fig. 1A). Moreover, its characteristic longitudinal and transverse surface plasmon absorption bands at 684 nm and 516 nm, respectively (Fig. 1B). Additionally, the electromagnetic field amplitude pattern of single AuNR from FDTD simulation (Fig. S3) indicated that the strongest EM field was along the sharp corner, which was similar to our previous work (Zhang et al., 2018), suggesting that the AuNRs with outstanding proprieties were achieved.

DFM technique is considered as a very powerful tool for the assay of disease biomarkers at single-particle level. The light scattering of AuNRs was observed at 652 nm (Fig. 1C), which displayed the red light scattering under dark-field microscope (Fig. 1D), and RGB analysis of the enlarged imaging proved that the average red percentage of light scattering imaging was more than 80% (Fig. 1E and F), which could act as a red light scattering probe for biochemical assay, such as the sensitive detection of cancer biomarkers under DFM.

3.3. Feasibility of this proposed strategy

To check the feasibility of the proposed strategy, the light scattering images of AuNRs were recorded under different condition (a-d in Fig. 2 A), which displayed red light scattering with differential intensity. The statistics result confirmed that the scattering intensities of AuNRs in the presence of I^- or H_2O_2 were scarcely changed (a-c in Fig. 2B). However, when both I^- and H_2O_2 were present, the obvious decrease in light scattering intensity of AuNRs was observed (d in Fig. 2B), suggesting that I^- and H_2O_2 were necessary for the chemical etching of AuNRs. Additionally, the AuNRs size statistics displayed an obvious decrease (Fig. S4), furthermore proved the chemical etching of AuNRs.

3.4. The validity verification of strand displacement amplification

The sensitive detection of miRNA-21 relied on strand displacement amplification, which was confirmed by polyacrylamide gel electrophoresis (Fig. S5). Lane 1–4 were miRNA-21, DNA 1, DNA 2, and fuel strand, which matched their molecular weights, respectively. In the presence of DNA 1 and DNA 2, they directly formed a double-stranded structure (lane 5) due to the base pairing. Furthermore, the fuel strand could hardly form duplexes with DNA 1 or DNA 2 and be unable to open the duplex structure between DNA 1 and DNA 2 when in the absence of miRNA-21 (lane 6). As displayed in lane 7, when the DNA 1, DNA 2 and miRNA-21 were simultaneously present, DNA hybrid complex were opened and DNA 2 were displacement by miR-NA-21. Likewise, when only DNA 1 and miRNA-21 (lane 8) or DNA 1 and Fuel (lane 9) were present, there were just the duplex products. However, lane 10 showed the only the target miRNA-21 could efficiently trigger this cycle reaction and quiet few DNA 2 were displacement as expected, which greatly amplified the signal. In this work, miRNA-21, DNA 2 and fuel strand presented the similar bases length, which presented the approximate molecular weights in the complexes or single-strands.

3.5. Conditions optimization for the highly detection of miRNA-21

In order to gain the best performance of this proposed strategy for miRNA-21 detection with high sensitivity and specificity, some crucial factors were optimized, Since the concentration of MBs exerted an influence on the scattering signal, excessive MBs would hinder the modification efficiency between MBs and DNA 1, leading to less DNA 1 strand modified on the surface of MBs. Thus, optimization of concentration of MBs was crucial for the detection of target miRNA. When the concentration of MBs was 0.5 mg/mL, the ratio of I/I_0 was similar to when the concentration of MBs was 1.5 mg/mL or 2.0 mg/mL (Fig. 3A), where, I was the light scattering intensity of the etched AuNRs and I_0 was the light scattering intensity of AuNRs before chemical etching. However, it reached minimum when the MBs was 1.0 mg/mL, thus, the 1.0 mg/mL chosen as the subsequent working conditions.

In this work, I_2 was formed by I^- and H_2O_2, which was further used to etch AuNRs. The lack of I^- obviously impacted the concentration of I_2, subsequently caused an unsatisfied sensitivity. Therefore, the concentration of I^- was essentially optimized. When the concentration of I^- was 1.0 mM, a great response was obtained, which could work as the optimized concentration (Fig. 3B). Furthermore, the etching reaction time and temperature dramatically affected the efficiency and sensitivity, and the result suggested that the incaution at 25 °C for 20 min was optimum for this work (Fig. 3C and D).

In addition, to obtain the best performance, other operation conditions were investigated. 200 ms exposure time for DFM image presented the optimal light scattering property of AuNRs (Fig. S6). Furthermore, the lack of acid or inadequate enzymatic incubation time is adverse to produce enough H_2O_2. When the concentration of HCl was 5 mM, or more than 10 mM, the I/I_0 was not satisfactory, thus 10 mM was

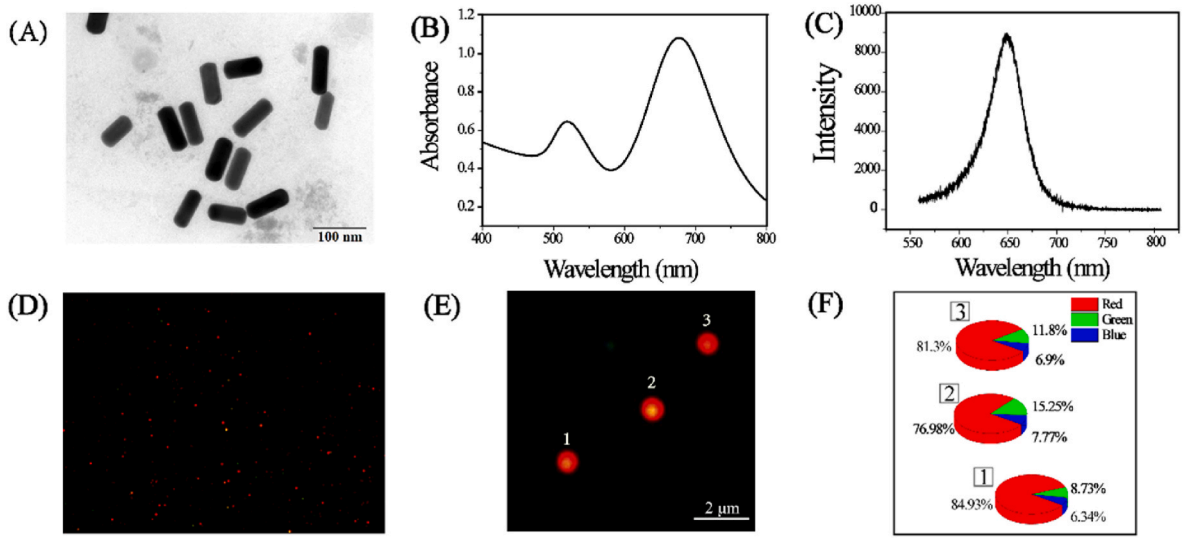

Fig. 1. The characterization of AuNRs. (A) The TEM image of AuNRs; (B) The UV-vis absorption spectrum of AuNRs; (C) The scattering spectrum of AuNRs; (D) The typical dark-field image of AuNRs, exposure time: 200 ms; (E) The enlarged image of three nanoparticles from (D); (F) the corresponding RGB analysis of three nanoparticles in (E).

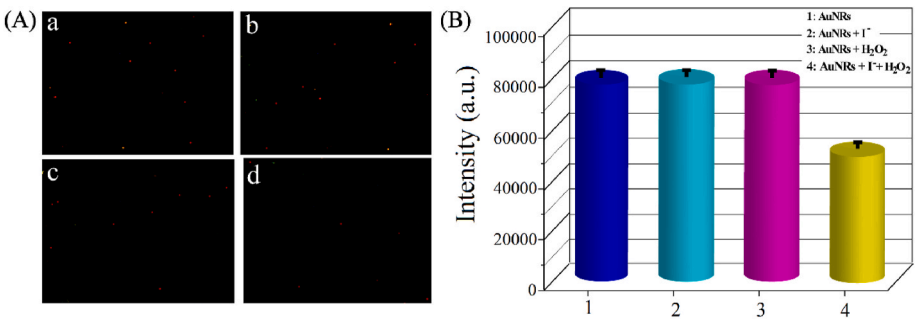

Fig. 2. (A) Dark-filed images obtained under the different conditions. (B) The scattering intensity of AuNRs under different conditions. (a) AuNRs; (b) AuNRs +1 mM I^-; (c) AuNRs +1 μM H_2O_2; (d) AuNRs +1 mM I^- + 1 μM H_2O_2. Condition: *c* (HCl), 10 mM; T $_{etching\ reaction}$, 25 °C; *t* $_{etching\ reaction}$, 20 min.

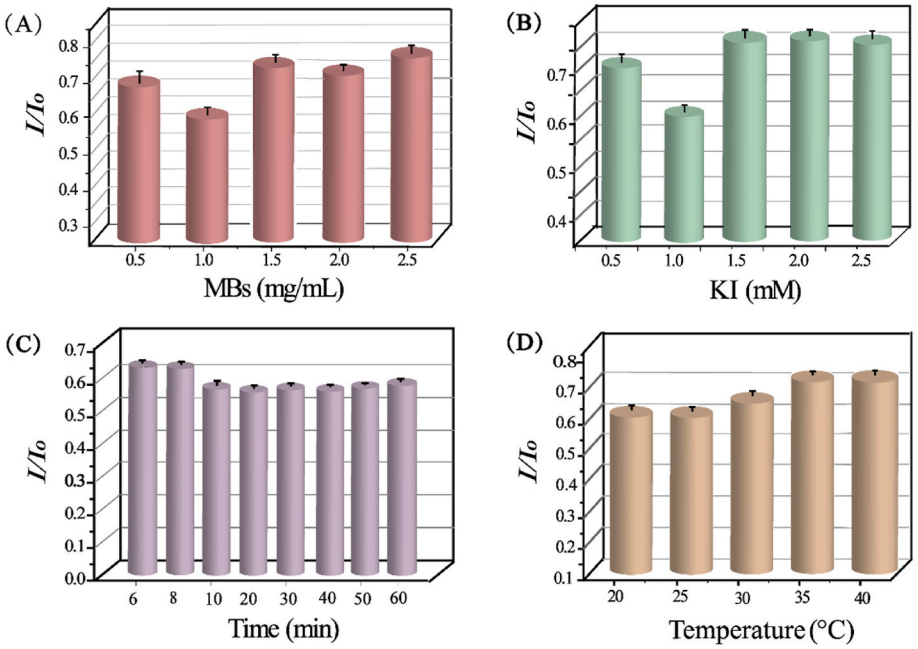

Fig. 3. (A) Optimization of MBs concentration; (B) Optimization of the concentration of I^-; (C) Optimization of reaction time; (D) Optimization of temperature. Conditions: *c* (GOx), 1 mg/mL; *c* (I^-), 1.0 mM; *c* (MBs),1.0 mg/mL; *c* (miRNA-21), 10 pM; T $_{etching\ reaction}$, 25 °C; *t* $_{etching\ reaction}$, 20 min; T $_{enzymatic\ reaction}$, 37 °C; *t* $_{enzymatic\ reaction}$, 40 min.

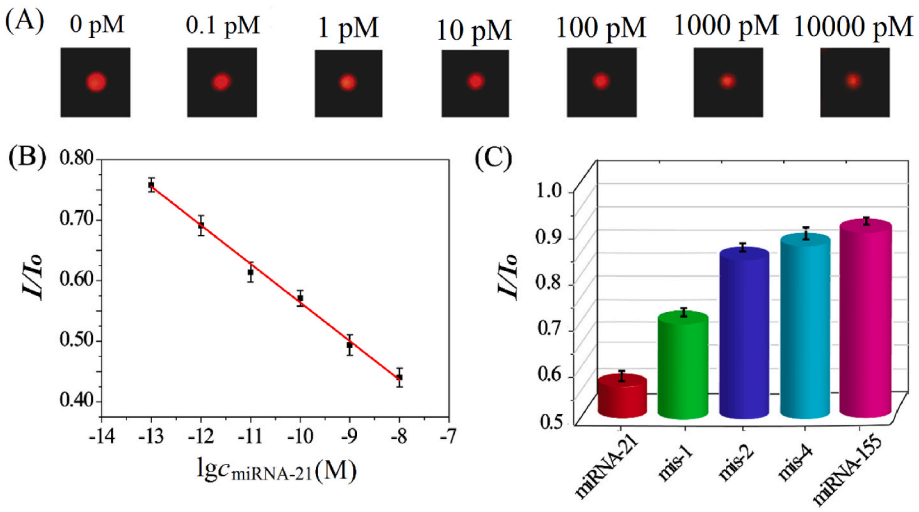

Fig. 4. The sensitivity and specificity for miRNA-21 detection. (A) The typical DFM images of AuNR with various concentration of miRNA-21. (B) The linear plot of scattering intensity ratio changes versus the miRNA-21 concentration. (C) Specificity investigation of the proposed method for different miRNA sequences, from left to right were target miRNA-21 (100 pM), single-base mismatch sequence (mis-1, 1000 pM), double-base mismatch sequence (mis-2, 1000 pM), four-base mismatch sequence (mis-4, 1000 pM) and miRNA-155 (1000 pM), respectively. Conditions: *c* (GOx), 1 mg/mL; *c* (I^-), 1.0 mM; *c* (MBs),1.0 mg/mL; *c* (miRNA-21), 0.1–10000 pM; T $_{etching\ reaction}$, 25 °C; T $_{enzymatic\ reaction}$, 37 °C; *t* $_{etching\ reaction}$, 20 min; *t* $_{enzymatic\ reaction}$, 40 min.

considered as the most suitable HCl concentration (Fig. S7). The inadequate enzymatic incubation time is adverse to produce enough H_2O_2, which reached a plateau when the incubation time was 40 min (Fig. S8), which was considered as the most suitable working condition.

Base on the above investigation, the optimal exposure time was 200 ms, the optimal concentration of MBs, I^- and HCl was 1.0 mg/mL, 1.0 mM, and 10 mM respectively. The chemical etching was carried out at 25 °C for 20 min and the enzymatic incubation reaction was performed at 37 °C for 40 min.

3.6. The sensitivity and specificity detection of miRNA-21

The above proposed functionalized conjugation can be developed as a sensing platform for miRNA-21 detection. Thus the sensing ability of this method was explored under the optimized condition. Typically, the different concentrations of miRNA-21 from 0.1 pM to 10,000 pM were introduced in this assay with a same performance operation (Fig. 4 A and B). Notably, the ratio of scattering intensity (I/I_0) the dark-field imaging highly improved the quantification sensitivity. A good linear relationship between the signal I/I_0 and the concentration of miRNA-21 was obtained with regression equation as $I/I_0 = -0.06375 \lg c_{\text{miRNA-21}}$ -0.07346 (c, M) with the correlation coefficient $R^2 = 0.9957$, and the limit of detection (LOD) was calculated to be 71.22 fM (3σ/k). However, if these samples were detected with U-3010 spectrophotometer, it showed a low sensitivity (Fig. S9). Moreover, Table S2 summarized a series of different methods for microRNA-21 assay, which proved that this plasmonic biosensor held remarkable sensitivity owing to the high resolution of dark-field microscopy.

Likewise, this plasmonic biosensor endowed a great specificity. Three different base mismatch sequences (mis-1, mis-2, mis-4), miRNA-155 and target miRNA-21 were performed for specificity investigation. Even though the concentration of interfering sequences were ten times higher than miRNA-21, other sequences, including mis-2, mis-4 and miRNA-155 scarcely responded, single base-mismatch just presented a little response. However, the target miRNA-21 was much high response conversely, suggesting the excellent specificity of this proposed platform.

3.7. The detection of microRNA-21 in human serum sample

In order to assess the practical application of this way, the human serum sample of three volunteers were chosen to explore the recovery efficiency assay. Different concentrations of miRNA-21 (with a final concentration of 50,100, 200 pM respectively) were spiked into the serum sample (Table 1). The result suggested that a satisfied recovery was obtained in the range of 103.68%–107.82%, and the relative standard deviation (RSD) results were between 1.28% and 8.05%, suggesting the remarkable specificity of the plasmonic biosensor.

4. Conclusions

In summary, the proposed strategy was able to detect target miRNA at an fM level and exhibited excellent specificity even a single-base mismatch sequence, owe to the strand displacement amplification and excellent LSPR and light scattering property of AuNRs. Besides, the satisfactory recoveries in human serum samples enable this strategy to hold a promising prospected in filed early diagnosis of diseases. Importantly, this proposed strategy could serve as a universal plasmonic platform by changing corresponding probe sequence and enzyme for other analysis applications.

Conflict of interest

The authors declare no competing financial interest.

Table 1
Results of human serum sample analysis (n = 3).

Added (pM)	Found (pM)	Average (pM)	Recovery (%)	RSD (%)
50.00	52.03 50.82 58.87	53.91	107.82	8.05
100.00	102.21 109.52 99.30	103.68	103.68	5.08
200.00	207.09 210.58 205.36	207.68	103.84	1.28

CRediT authorship contribution statement

Qiang Zhang: Investigation, Formal analysis, Data curation, Writing – original draft. **Hong Hui Yan:** Investigation, Conceptualization. **Cheng Ru:** Conceptualization. **Fu Zhu:** Conceptualization. **Hong Yan Zou:** FDTD simulation. **Peng Fei Gao:** Conceptualization. **Cheng Zhi Huang:** Conceptualization. **Jian Wang:** Supervision, Methodology, Conceptualization, Writing – review & editing, Funding acquisition.

Declaration of competing interest

The authors declare that no competing financial interests that could hinder the work reported in this paper.

Acknowledgments

This work was supported by the National Natural Science Foundation Project of China (No. 22174115), the Natural Science Foundation Project of Chongqing (cstc2019jcyjmsxmX0279), and the Fundamental Research Funds for the Central Universities (XDJK2019AC002).

Appendix A. Supplementary data

Supplementary data to this article can be found online at https://doi.org/10.1016/j.bios.2021.113942.

References

Chen, Z., Li, J., Chen, X., Cao, J., Zhang, J., Min, Q., Zhu, J.-J., 2015. J. Am. Chem. Soc. 137 (5), 1903–1908.
Dai, Y., Furst, A., Liu, C.C., 2019. Trends Biotechnol. 37 (12), 1367–1382.
Fu, J., Liu, M., Liu, Y., Woodbury, N.W., Yan, H., 2012. J J. Am. Chem. Soc. 134 (12), 5516–5519.
Gao, P.F., Lei, G., Huang, C.Z., 2021. Anal. Chem. 93 (11), 4707–4726.
Jin, T., Zhang, J., Zhao, Y., Huang, X., Tan, C., Sun, S., Tan, Y., 2020. Biosens. Bioelectron. 150, 111936.
Li, M.-X., Xu, C.-H., Zhang, N., Qian, G.-S., Zhao, W., Xu, J.-J., Chen, H.-Y., 2018. ACS Nano 12 (4), 3341–3350.
Li, Q., Peng, M., Wang, C., Li, C., Li, K., Lin, Y., 2019. ACS Sustain. Chem. Eng. 7 (24), 19338–19343.
Li, T., Wu, X., Liu, F., Li, N., 2017. Analyst 142 (2), 248–256.
Li, Y., Jing, C., Zhang, L., Long, Y.-T., 2012. Chem. Soc. Rev. 41 (2), 632–642.
Li, Y., Li, K., Liu, Q.-Y., Chen, Z., 2020. ACS Sustain. Chem. Eng. 8 (11), 4555–4560.
Liu, J.J., Yan, H.H., Zhang, Q., Gao, P.F., Li, C.M., Liang, G.L., Huang, C.Z., Wang, J., 2020a. Anal. Chem. 92 (19), 13118–13125.
Liu, M., Mao, X., Huang, L., Fan, C., Tian, Y., Li, Q., 2020b. Anal. Chem. 92 (1), 1333–1339.
Liu, X., Zhang, S., Tan, P., Zhou, J., Huang, Y., Nie, Z., Yao, S., 2013. Chem. Commun. 49 (18), 1856–1858.
Markou, A., Tsaroucha, E.G., Kaklamanis, L., Fotinou, M., Georgoulias, V., Lianidou, E.S., 2008. Clin. Chem. 54 (10), 1696–1704.
Ouyang, T., Liu, Z., Han, Z., Ge, Q., 2019. Anal. Chem. 91 (5), 3179–3186.
Shi, L., Jing, C., Ma, W., Li, D.-W., Halls, J.E., Marken, F., Long, Y.-T., 2013. Angew. Chem. Int. Ed. 52 (23), 6011–6014.
Sun, H., Yao, F., Su, Z., Kang, X.-F., 2020. Hybridization chain reaction (HCR) for amplifying nanopore signals. Biosens. Bioelectron. 150, 111906.
Tian, T., Zhao, J., Wang, Y., Li, B., Qiao, L., Zhang, K., Liu, B., 2021. Biosens. Bioelectron. 178, 113003.
Wang, F., Li, Y., Han, Y., Ye, Z., Wei, L., Luo, H.B., Xiao, L., 2019a. Anal. Chem. 91 (9), 6329–6339.
Wang, G., Guo, Y., Liu, Y., Zhou, W., Wang, G., 2021a. ACS Sens. 6 (3), 958–966.

Wang, H., Xu, C.-H., Zhao, W., Chen, H.-Y., Xu, J.-J., 2021b. Anal. Chem. 93 (30), 10727–10734.
Wang, H., Zhao, W., Xu, C.-H., Chen, H.-Y., Xu, J.-J., 2019b. Chem. Sci. 10 (40), 9308–9314.
Wu, L., Qu, X., 2015. Chem. Soc. Rev. 44 (10), 2963–2997.
Wu, S., Ma, C., Gao, Y., Su, Y., Xia, Q., Chen, Z., Zhu, J.-J., 2020. Anal. Chem. 92 (14), 9940–9947.
Xianyu, Y., Lin, Y., Chen, Q., Belessiotis-Richards, A., Stevens, M.M., Thomas, M.R., 2021. Angew. Chem. Int. Ed. 60 (18), 9891–9896.
Xu, S., Yu, X., Chen, Z., Zeng, Y., Guo, L., Li, L., Luo, F., Wang, J., Qiu, B., Lin, Z., 2020. Anal. Chem. 92 (13), 9016–9023.
Yan, H.H., Zhang, Q., Cheng, R., Zhu, F., Liu, J.J., Gao, P.F., Zou, H.Y., Liang, G.L., Huang, C.Z., Wang, J., 2021. ACS Appl. Bio Mater. 4 (3), 2849–2854.
Zhan, X., Yang, S., Huang, G., Yang, L., Zhang, Y., Tian, H., Xie, F., Lamy de la Chapelle, M., Yang, X., Fu, W., 2021. Biosens. Bioelectron. 188, 113314.
Zhang, N., Shi, X.M., Guo, H.Q., Zhao, X.Z., Zhao, W.W., Xu, J.J., Chen, H.Y., 2018. Anal. Chem. 90 (20), 11892–11898.
Zhao, Y., Gao, X.-Y., Wang, H., Wang, J., Zhou, J., Zhao, W., Xu, J.-J., Chen, H.-Y., 2019. Anal. Chem. 91 (24), 15988–15992.